Princeton Plasma Physics Laboratory

PPPL-

PPPL-

![PPPL Princeton Plasma Physics Laboratory logo]

Princeton Plasma Physics Laboratory
Report Disclaimers

PPPL Report Availability

Princeton Plasma Physics Laboratory:

http://www.pppl.gov/techreports.cfm

Office of Scientific and Technical Information (OSTI):

http://www.osti.gov/bridge

Related Links:

U.S. Department of Energy

Office of Scientific and Technical Information

Fusion Links

Simulation of Localized Fast-Ion Heat Loads in Test Blanket Module Simulation Experiments on DIII-D

G.J. Kramer[1],[*] A. McLean[2], N. Brooks[3], R.V. Budny[1], X. Chen[4],

W.W. Heidbrink[4], T. Kurki-Suonio[5], R. Nazikian[1], T. Koskela[5],

M.J. Schaffer[3], K. Shinohara[6], J.A. Snipes[7], and M.A. Van Zeeland[3]

[1]*Princeton Plasma Physics Laboratory,*

P.O.Box 451, Princeton, New Jersey 08543

[2]*Lawrence Livermore National Laboratory, Livermore, CA 94550, USA*

[3]*General Atomics, P.O. Box 85608, San Diego, CA 92186, USA*

[4]*University of California-Irvine, Irvine, CA, USA*

[5]*Helsinki University of Technology, Helsinki, Finland*

[6]*JAEA, 801-1, Mukouyama, Naka City, Ibaraki, 311-0193, Japan and*

[7]*ITER Organization, Route de Vinon sur Verdon,*

13115 St. Paul lez Durance, France

(Dated: September 12, 2013)

Abstract

Infrared imaging of hot spots induced by localized magnetic perturbations using the Test Blanket Module (TBM) mock-up on DIII-D is in good agreement with beam-ion loss simulations. The hot spots were seen on the carbon protective tiles surrounding the TBM as they reached temperatures over 1000 C. The localization of the hot spots on the protective tiles is in fair agreement with fast-ion loss simulations using a range of codes: ASCOT, SPIRAL, and OFMCs while the codes predicted peak heat loads that are within 30% of the measured ones. The orbit calculations take into account the birth profile of the beam ions as well as the scattering and slowing down of the ions as they interact with the localized TBM field. The close agreement between orbit calculations and measurements validate the analysis of beam ion loss calculations for ITER where ferritic material inside the tritium breeding TBMs is expected to produce localized hot spots on the first wall.

[*]gkramer@pppl.gov

FIG. 1: The four protective carbon tiles on the DIII D TBM mock-up assembly (left). The (a) radial, (b) vertical, and (c) toroidal magnetic field components generated by the TBM mock-up in DIII-D on the mid-plane at the low-field side plasma edge.

I. INTRODUCTION

Tritium breeding is of paramount importance for a viable fusion reactor. As part of the ITER mission tritium breeding will be studied in six Test Blanket Modules (TBMs) which will be mounted pair-wise in three equatorial ports. These TBMs contain a significant amount of ferritic steel, and therefore, the TBMs will create three highly localized distortions of the magnetic field which can reduce the confinement of fast ions, especially the fusion-born alpha particles. It was shown from alpha-particle confinement simulations for ITER that a substantial fraction of the lost alpha particles is deposited on the surface of the TBMs thereby creating hot spots [1–4].

During TBM experiments in DIII-D [5] in which a scaled mock-up of the magnetic error field of a pair of typical TBMs in one ITER port was placed in the machine, the confinement of fast beam-ions was studied. The mock-up TBM on DIII-D has four protective carbon tiles arranged vertically with a thermocouple placed on the back of each 2.5 cm thick tile (Fig. 1). In a first series of experiments (in 2009) the thermocouple signals were used to deduce fast-ion induced heat loads on the surface of the tiles [4]. This involved modeling of the fast-ion losses to the TBM tiles in the presence of a highly localized error field near the TBM mock-up (Fig. 1) and the modeling of the heat transport through the tiles. Although good agreement between the measured and modeled thermocouple temperature response was found, there were still questions about possible heat load contributions from the thermal plasma and of the precise shape of the hot spot on the tiles. In those studies four fast-ion transport codes were used, the ASCOT code [6], the DELTA5D Monte Carlo code [7], the OFMC code [8, 9] and the SPIRAL code [10]. The codes gave very similar answers for the total power deposited in the TBM hot spots coming from particles deposited near the plasma edge ($r/a > 0.7$) [4], but the details on the size, shape, and peak heat loads of the spot were different. Those differences in the fast-ion loss simulations can be resolved by measuring the hot spot on the tiles directly with an Infra Red (IR) thermal imaging camera. In this paper

the results of IR imaging experiments which were performed last year are reported.

First, the alternate explanation for the heat loads, thermal plasma moving close enough to the tiles when the TBM fields are engaged and so contributing to the thermal heat load, is investigated and ruled out based on the thermal images (Sec. II). Once it was established that the heat loads were completely due to TBM-induced beam-ion losses, we have injected the various beams in DIII-D separately to measure the TBM hot spot for different pitch angle distributions (Sec. II). Those pitch-angle resolved losses are compared with results from three fast-ion loss simulation codes (ASCOT, OFMC, and SPIRAL) that can propagate the particles to the DIII-D wall (Sec. III). From a favorable comparison between the the experiments and simulations as discussed in Sec. IV it is concluded that the fast-ion loss codes can be used to estimate heat loads on the TBM surfaces in ITER (Sec. V).

II. EXPERIMENTS

In three similar discharges the thermal plasma contribution to the tile heating was investigated. Those discharges had a toroidal magnetic field of 1.7 T, a plasma current of 1.2 MA, a central electron density of 3.7×10^{19} m^{-3}, and a maximum electron temperature of 2.7 keV. The plasmas were ELMy H-mode plasmas with a gap of 4.4 cm between last closed flux surface and the TBM tiles. In all the experiments presented in this paper the TBM coils were operated at their maximum current to create an error field that is three times larger than expected in ITER [5] for maximum losses.

In the first discharge 2 MW of Neutral Beam Injection (NBI) was used without TBM fields. No heating of the TBM tiles was observed with the IR camera, sampled at 1.6 kHz, as can be seen in Fig. 2a. In the second discharge the TBM fields were engaged during the 2 MW NBI heating phase. This resulted in a significant heating of the tiles (Fig. 2b). In the third discharge the NBI was replaced by 3.3 MW of Electron Cyclotron Heating (ECH) while the TBM fields were engaged. No significant heating of the TBM tiles was observed as can be seen in Fig. 2c.

Those experiments demonstrate that beam-ions in combination with the TBM fields produce the observed hot spots on the TBM protective tiles in DIII-D and not the interaction between thermal plasma and the TBM tiles when the TBM fields are present. They also confirm the interpretation given in [4] of the TBM tile temperature rise as caused by fast-ion

3

FIG. 2: Heat loads in similar discharges: (a) 2 MW of NBI without TBM fields, (b) 2 MW of NBI with TBM fields, and (c) 3.3 MW ECRH with TBM fields showing that only the combination of TBM fields and fast ions from NBI injection creates a hot spot on the TBM tiles.

FIG. 3: The lay-out of the various beams in DIII-D. Beam lines in red were used in the current experiments. The pitch distribution created by the various beam lines.

losses to the protective TBM tiles.

We can utilize the TBM error fields in combination with NBI injection from various beam lines, shown in Fig. 3, as a sensitive tool to benchmark fast-ion loss simulation codes by comparing the simulated heat loads with measured ones from the IR imaging. Particles from different beams have characteristic pitch distributions (Fig. 3) whereby the pitch is defined as $v_\parallel/v$ with v the particle velocity and $v_\parallel$ parallel to the magnetic field line and a positive sign is defined in the direction of the plasma current. By injecting the beams separately pitch dependence of the TBM induced losses was obtained.

During a DIII-D discharge (shot #147603) which was very similar to the discharges used in the fast-ion heating studies, the TBM coils were engaged for 2 s during the stationary flat top phase of the discharge while the 030L beam was injected at half power, which was achieved by modulating the beam with a 10 ms on 10 ms off duty cycle, to keep the plasma in H-mode, the other beams were injected one by one for 180 ms in 350 ms periods During each 180 ms injection period a full slowing-down distribution is created (the fast-ion energy slowing-down time is about 60 ms) followed by a period where the slowing-down distribution thermalizes. In this way the heat loads from successive beams on the TBM tiles was measured in a single discharge. The gap between the TBM surface and the last closed flux surface was kept at 4.2 ±0.4 cm with a steady H-mode density profile.

Heat loads on the TBM tiles were obtained from the measured IR temperature data by using the THEODOR 2-D analysis code [11]. The thermal analysis included temperature dependent heat diffusion and conduction coefficients for the ATJ graphite while a loosely adhered surface layer was taken into account with a heat transmission coefficient of

power deposited on TBM tiles [kW]

DIII-D beam experiment	ASCOT	OFMC	SPIRAL
030R + 0.5 030L	90.2	50.7	66.5	44.9
210L + 0.5 030L	107.7	44.1	72.7	71.9
0.5 030L	48.1	13.1	13.6	14.8
330L + 0.5 030L	59.3	56.1	45.5	33.2
210R + 0.5 030L	92.0	56.5	46.5	39.6

TABLE I: The power deposited in the hot spot on the TBM tiles in the experiment and as calculated by the ASCOT, OFMC, and SPIRAL codes. Typical uncertainties in the experimental values are 30%.

5 MW/m^2/K. In the heat load analysis care was taken not to include the increased heat loads due to ELMs. The power that was deposited onto the TBM surface was obtained by integrating the heat load over all the four tiles and is given in the second column of Table I while the measured heat loads are shown in the left-hand side columns of Figs. 4 and 5 for the tangential and perpendicular beams, respectively, and for the half beam in Fig. 6.

The total power that is deposited on the TBM tiles by the perpendicular counter-going beam (210L) is almost 20% higher than the equivalent co-going beam (030R). The same holds for the tangential beams (co-going: 330L, counter-going: 210R), with an increase in measured heat load from co- to counter injection of 55%. It was expected that the deposited power is higher for the counter injected beams because beam neutrals that are ionized near the plasma edge are born on trapped orbits. For the co-injected beams the ions are born on the outside leg of their orbit and after bouncing those ions will traverse the central part of the plasma on their inside leg while for the counter-injected beams the ions are born on the inside leg of their orbit and after bouncing they will have their outside leg further out to the edge and beyond.

The perpendicular beams (030R and 210L) deposit a higher amount of power (up to 25%) on the tiles than the tangential beams (330L and 210R) which can be understood from the fact that the perpendicular beams generate more trapped particles at the edge which are more sensitive to the TBM error fields.

The power deposition from the half co-going beam (030L) is rather puzzling. When this beam is injected alone it apparently delivers 48.1 kW onto the TBM tiles, while injected

FIG. 4: Measured heat loads (left column) compared to heat loads as calculated with the ASCOT (second), OFMC (third), and SPIRAL (last column) codes for the co- and counter going tangential injected beams. For each frame the peak heat load is given.

FIG. 5: Measured heat loads (left column) compared to heat loads as calculated with the AS-COT (second), OFMC (third), and SPIRAL (last column) codes for the co- and counter going perpendicular injected beams. For each frame the peak heat load is given.

together with the 330L beam, which has the same beam geometry as the 030L beam, the power deposition only increases by 11.2 kW. Contrary to the expectation that the 030L half beam would deposit half as much power as the 330L full beam, it deposits more than four times the power of the full beam.

III. PARTICLE-LOSS AND HEAT-LOAD SIMULATIONS

Beam-ion transport was calculated with three different codes: the OFMC code which is guiding-center following code and the ASCOT and SPIRAL codes which are full-orbit following codes. All three codes use an axisymmetric EFIT equilibrium [12] with the full 3-D vacuum ripple field induced by the TBM superimposed on it. The TBM field has a high dominant toroidal mode number, $n = 9$, and therefore, resonant shielding is negiglible because the resonant condition: $m - nq = 0$, is not met which justifies the vacuum field approach. All three codes solve for the trajectories of the same ensemble of 50000 particles

FIG. 6: Measured heat loads (left column) compared to heat loads as calculated with the ASCOT (second), OFMC (third), and SPIRAL (last column) codes for the co-injected tangential beams with 50% duty cycle. For each frame the peak heat load is given.

6

FIG. 7: The shape of the TBM tiles used in the ASCOT modeling. The same shape was used in the OFMC and SPIRAL codes. The yellow outline indicates the location of the TBM coils behind the protective tiles.

for each beam drawn from the actual toroidally asymmetric beam deposition profiles as calculated by TRANSP/NUBEAM [13] codes with initial energies varying between 74 and 80 keV depending on the used NBI source. This removes the uncertainty on the birth profiles when the results from the different codes are compared. Three of the five beams were injected in the co-current direction (030L, 030R, and 330L) while the other two (210L, and 210R) were injected in the counter-current direction resulting in anisotropic pitch distributions as shown in Fig. 3. The particles were followed beyond the separatrix to the first wall and the TBM tiles that are at R=2.377 m which is the same radius at the outer wall. In all three codes the three poloidal limiters at 95, 230, and 310 deg. were included together with an accurate model of the TBM tiles that included the beveled tile shape and the space of the port next to the tiles as can be seen in Fig. 7 for the ASCOT code.

Slowing down and collisions [14] were included in all the codes and particles were followed until they reached thermal velocities or got lost to the wall. In the following we will compare the simulation results of the different codes as the sum of the full injected beams (030R, 210L, 210R, and 330L) and the half beam (030L) with each other first. This is then followed by a comparison of the simulations with the experimental results.

A. comparison between codes

All three codes show the formation of a hot spot on the central two TBM tiles as shown in Figs. 4, 5, and 6 which is in agreement with the measurements. The total power deposited in the hot spot on the TBM tiles varies somewhat between the different codes. OFMC and SPIRAL show the highest power deposited for the counter-going perpendicular beam (210L) while ASCOT predicts significant lower losses from that beam. Both OFMC and SPIRAL show enhanced losses from the counter-going perpendicular beam (210L) compared to the co-going perpendicular beam (030R) which can be explained by enhanced prompt losses due to the counter-injection. ASCOT does not find those enhanced counter-injection losses

7

FIG. 8: Measured peak heat loads compared to peak heat loads as calculated with the ASCOT, OFMC, and SPIRAL codes for the five used beams.

FIG. 9: Measured deposited power on the TBM tiles compared to the deposited power as calculated with the ASCOT, OFMC, and SPIRAL codes for the five used beams.

for the perpendicular beams. All three codes agree well on the power that is deposited by the continuous half beam (030L). ASCOT and OFMC both find that the deposited power for the co- and counter tangential beams (330L and 210R) are the same although OFMC predicts less power than ASCOT while SPIRAL finds about 20% more losses from the counter injected tangential beam (210R) compared to the co-injected tangential beam (330L). The power deposited on the TBM tiles from tangential injection as calculated with the SPIRAL code is less than the power deposited as calculated with ASCOT and OFMC codes.

All three codes predict slightly different hot-spot foot prints on the TBM tiles as can be seen in Figs. 4, 5, and 6. In combination with the differences in deposited power, it is not surprising to find variations in the peak heat loads as shown in Fig. 8. In most cases the OFMC code gives the highest peak heat load which occurs at the transition between the flat surface and the beveled edge that faces the plasma current. For the co- and counter perpendicular beams (030R and 210L) both OFMC and SPIRAL find the highest peak heat loads for the counter injected beam (210L) while ASCOT finds the opposite. Peak heat loads from the co- and counter tangential beams (330L and 210R) are found to be similar for OFMC and ASCOT while the SPIRAL peak heat loads are lower than the ASCOT and OFMC results.

B. comparison with experiment

The three codes reproduce the peak heat fluxes well for the four continuously injected beams as can be seen in Fig. 8 while the peak heat loads for the half beam are severely underestimated by all the simulations. The simulated foot prints of the hot spots compare

8

in general well with the measured foot prints (Figs. 4, 5, 6) although the simulated foot prints are more fuzzy at the edges and sometimes somewhat smaller than the measured ones.

The codes underestimate the measured total power deposition on the TBM tiles as is shown in Fig. 9 and table I. The origine of this discrepancy, as discussed below, can be due to plasma effects that are not accounted for in the simulations and/or due to the analysis method for extracting heat loads from the measured temperatures.

IV. DISCUSSION

The first obvious reason why the 030L beam can give a higher heat load is shine-through of the beam that hits the area where the TBM is located as can be seen in Fig. 3. This possibility can be ruled out because the shine-through is less than 0.5% in those plasmas and it is deposited over a much wider area than the TBM tiles. An estimate of the shine-through heat load is less than 50 kW/m^2 and should have shown up as a uniform back-ground on the TBM tiles and surrounding armour (Fig. 2) if the IR camera was sensitive enough to register those low heat loads.

Turbulence and low levels of MHD activity, which were not included in the simulations, can increase the fast-ion transport from the plasma core and induce extra losses. The discharges that were used in this study were selected for their low MHD activity and therefore, enhanced losses from this mechanism are expected to be negligible. Increased heat loads due to ELMs were observed in the IR camera data but omitted from the reported experimental results.

It has previously been shown experimentally and from simulations that the heat loads and power depositions are very sensitive to the gap between the last-closed surface and the TBM tiles [4]. When this gap is decreased in the simulations so that the simulated deposited power agrees with the measured deposited power, it does not solve the problem: decreasing the gap will result in much higher peak heat loads in the simulations than the observed ones.

An alternative explanation for the discrepancy between the measured and simulated power deposition might be found in the way the deposited power is obtained. In both the experiment and simulations the deposited power was obtained by integrating the heat loads over the four TBM tiles. In the simulations the heat load is solely caused by fast ions

impacting on the TBM surface. In the experiments, however, the heat load is determined from the measured change in tile temperature in combination with the well known material properties of the ATJ graphite tiles. On time scales that are short compared to the heat conduction timescale the measured rise in temperature is caused by the heat flux from the impinging particles. On longer time scales the measured temperature rise, and hence, the deduced heat load, is caused by both the fast ion power deposition on the tiles and from heat conduction through the tile. The source of the power that is conducted through the tiles is the power that was deposited earlier in the fast-ion induced hot spot. The direct fast-ion power deposition cannot be separated experimentally from the heat conduction except at the hottest spot on the tile. The heat load at the hottest spot on the tile is solely caused by the fast ions because the heat can only diffuse away from that location. Therefore, the measured peak heat loads are only caused by the fast ions lost at that location and the simulated peak heat loads should (and do) agree with the measured ones.

Away from the maximum temperature location, both the fast ion deposition and the heat conduction through the tile contribute to the measured temperature rise and therefore, the experimental heat load is a combination of the fast-ion loss heat load and the apparent heat load due to conduction. The experimental power deposited on the tiles as calculated from the integration of the heat load is therefore the sum of the true heat load due to the fast-ion losses and the apparent heat load due to conduction through the tile. In the simulations only the power deposited by the fast-ions is obtained which is lower than the experimental power deposition that includes both the fast-ion and conductive heat loads.

V. CONCLUSION

Thermal imaging experiments of the protective TBM tiles in DIII-D have shown that the magnetic fields generated by a scaled mock-up of two TBMs for ITER create a hot spot on the two central carbon tiles that protect the TBM surface when NBI was injected. It was shown that this hot spot only appears with the TBM fields present during NBI injection and therefore, it was concluded that the hot spot is due to fast-ion losses. This was corroborated by fast-ion loss simulations.

In a systematic scan of the different beam lines in DIII-D which corresponds to varying the fast-ion pitch distribution, peak heat loads between 7 and 9 MW/m^2 were found for

four beams that were injected continuously at 2 MW. By integrating the heat loads over the TBM tile surfaces deposited powers between 50 and 110 kW were found. Those powers are most likely an overestimate of the power deposited by the fast ions because the IR camera measurements cannot distinguish between temperature changes due to fast-ion losses and heat conduction along the surface of the tiles. An anomalous high heat load was found when a single 2 MW modulated (10 ms on, 10 ms off) tangential beam was injected. Those high heat loads are not yet understood from fast-ion loss simulations.

Beam-ion loss calculations with different fast-particle orbit-following codes confirmed that the observed heating of the two central tiles is caused by beam-ion losses. The size and shape of the calculated hot spots agreed well for all three codes. Simulated peak heat loads were in general found within 30% of the observed ones, giving some confidence in using the fast-ion transport codes for estimating heat loads on the TBM modules in ITER. The total power deposited on the tiles was calculated to be lower than the experimental values because the simulations only give the power deposited by the fast ions whereas in the experiments some additional apparent heat load was included due to conduction along the the surface.

In ITER the fast ions are created by fusion reactions in the plasma core and to a lesser extent by NBI injection. In a previous study on DIII-D of the fast ion confinement in the presence of the TBM fields it was found and confirmed in the present experiments that that the core confinement was not affected by the TBM fields [4]. Extrapolating the results from the current DIII-D experiments to ITER, however, needs some caution. The TBM fields in DIII-D were chosen in such a way that DIII-D represented a scaled-down version of ITER [5]. In such a scaling, however, the fast-ion parameters such as the slowing-down time and critical energy don't scale into the range of the ITER parameters. In the DIII-D experiments the fast ions were injected close to the critical energy in contrast to the fusion-born alpha particles in ITER which are well above the critical energy. Similarly, the slowing-down time of the fast ions in DIII-D is on the order of 100 ms while the slowing-down time for fusion-born alpha particles in ITER is typically longer than one second. In the DIII-D experiments the particle distirbution was highly anisotropic and particles with with a small pitch were missing from the distribution (fig. 3). In ITER, however, the fusion-born alpha distribution is isotropic and a fraction of the alpha particles is born inside the loss cone near zero pitch may therefore contribute significantly to the heat load on the TBM tiles.
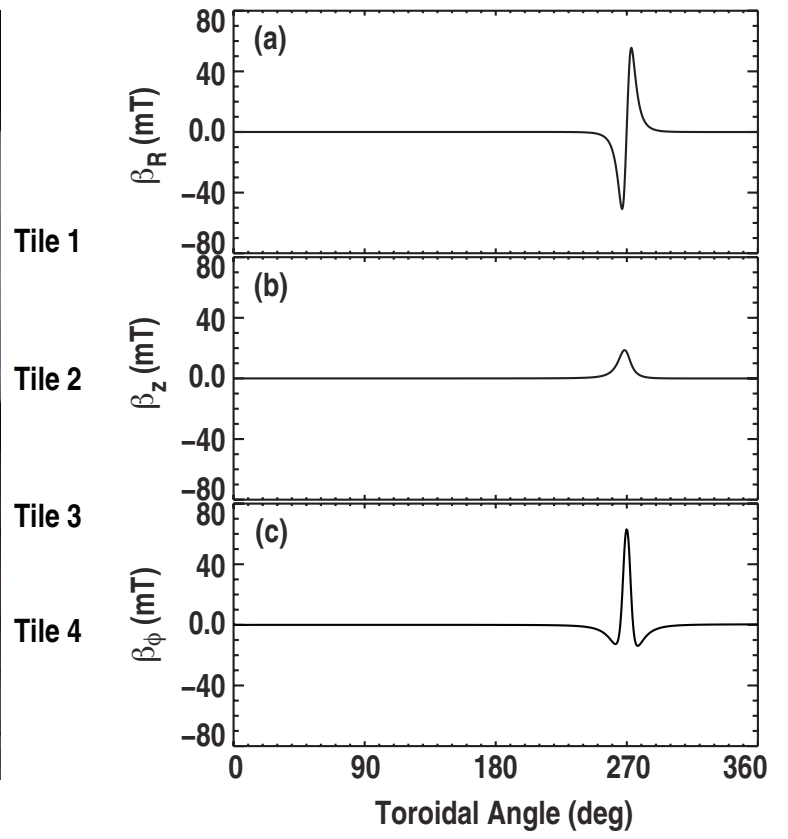
It was shown that the fast-ion loss codes can reproduce the heat load results for the

DIII-D experiments rather well, usually within 30% of the measured values, and therefore, those codes can be used with some confidence to predict heat loads on the TBM tiles in ITER in the design phase to avoid possible damage due to high heat loads.

[1] G.J. Kramer, R.B. White, R. Nazikian, and H.L. Berk, Fusion Energy Conference 2008 (Proc. 22nd Int. Conf., Geneva, 2008) CD-ROM file IT/P6-3, http://www-pub.iaea.org/MTCD/Meetings/FEC2008/it_p6-3.pdf

[2] T. Kurki-Suonio, O Asunta, T. Hellsten, V. Hynönen, T. Johnson, T. Koskela, J. Lönnroth, V. Parail, M. Roccella, G. Saibene, A. Salmi and S. Sipilä (2009) Nucl. Fusion **49**, 095001

[3] K. Shinohara, T. Kurki-Suonio, D. Spong, O. Asunta, K. Tani, E. Strumberger, S. Briguglio, T. Koskela, G. Vlad, S. Günter, G Kramer, S Putvinski, K Hamamatsu and ITPA Topical Group on Energetic Particles (2011) Nucl. Fusion **51**, 063028

[4] G.J. Kramer, R.V. Budny, R. Ellis, M. Gorelenkova, W.W. Heidbrink, T. Kurki-Suonio, R. Nazikian, A. Salmi, M.J. Schaffer, K. Shinohara, J.A. Snipes, D.A. Spong, T. Koskela, and M.A. Van Zeeland, (2011) Nucl. Fusion **51**, 103029

[5] M.J. Schaffer, J.A. Snipes, P. Gohil, P. de Vries, T.E. Evans, M.E. Fenstermacher, X. Gao, A.M. Garofalo, D.A. Gates, C.M. Greenfield, W.W. Heidbrink, G.J. Kramer, R.J. La Haye, S. Liu, A. Loarte, M.F.F. Nave, T.H. Osborne, N. Oyama, J.-K. Park, N. Ramasubramanian, H. Reimerdes, G. Saibene, A. Salmi, K. Shinohara, D.A. Spong, W.M. Solomon, T. Tala, Y.B. Zhu, J.A. Boedo, V. Chuyanov, E.J. Doyle, M. Jakubowski, H. Jhang, R.M. Nazikian, V.D. Pustovitov, O. Schmitz, R. Srinivasan, T.S. Taylor, M.R. Wade, K.-I. You, L. Zeng and the DIII-D Team, (2011) Nucl. Fusion **51**, 103028

[6] J.A. Heikkinen and S.K. Sipilä, (1995) Phys. of Plasmas **2**, 3724

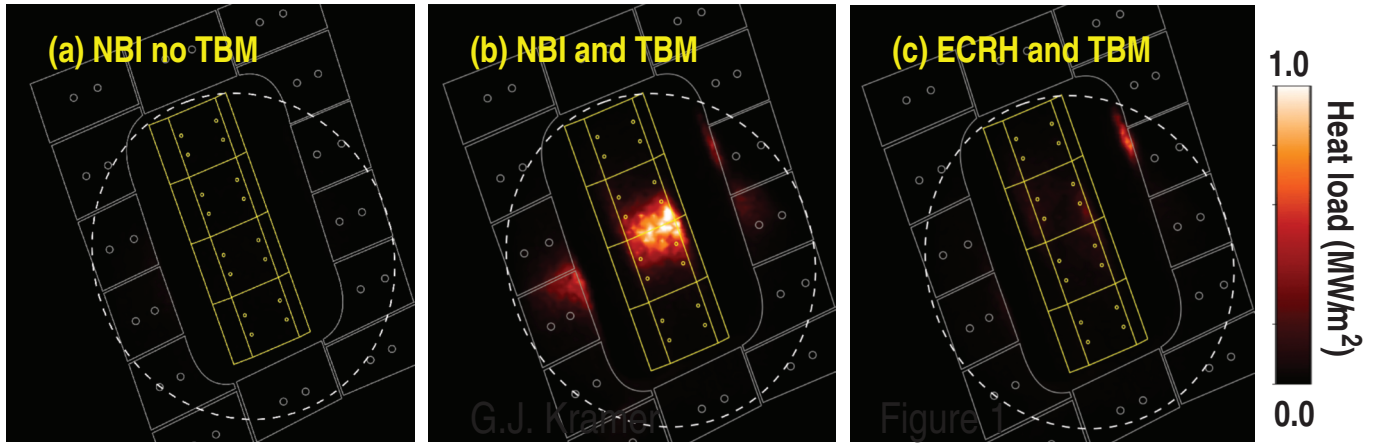[7] D.A. Spong, S.P. Hirshman, and J.C. Whitson, (1997) Plasma Phys. Rep., **23**, 483

[8] K. Tani, M. Azumi, H. Kishimoto, and S. Tamura (1981) Journal of Phys. Soc. Jpn. **50**, 1726

[9] K. Shinohara, H. Kawashima, K. Tsuzuki, K. Urata, M. Sato, H. Ogawa, K. Kamiya, H. Sasao, H. Kimura, S. Kasai, Y. Kusama, Y. Miura, K. Tobita, O. Naito, the JFT-2M Group and D.S. Darrow (2003) Nucl. Fusion **43**, 586

[10] G.J. Kramer, R.V. Budny, A. Bortolon, E.D. Fredrickson, G.Y. Fu, W.W. Heidbrink, R. Nazikian, E. Valeo,and M.A. Van Zeeland (2013) Plasma Phys. and Contr. Fusion **55**, 025013

[11] A. Herrmann, (2002) Plasma Physics and Contr. Fus. **44**, 883

[12] L.L. Lao, J.R. Ferron, R.J. Groebner, W. Howl, H. St. John, E.J. Strait, and T.S. Taylor, (1990) Nucl. Fusion **30**, 1035

[13] R.V. Budny, M.G. Bell, A.C. Janos, D.L. Jassby, L.C. Johnson, D.K. Mansfield, D.C. McCune, M.H. Redi, J.F. Schivell, G. Taylor, T.B. Terpstra, M.C. Zarnstorff and S.J. Zweben (1995) Nucl. Fusion **35**, 1497

[14] A.H. Boozer and G. Kuo-Petravic, (1981) Phys. Fluids **24**, 851

Tile 1

Tile 2

Tile 3

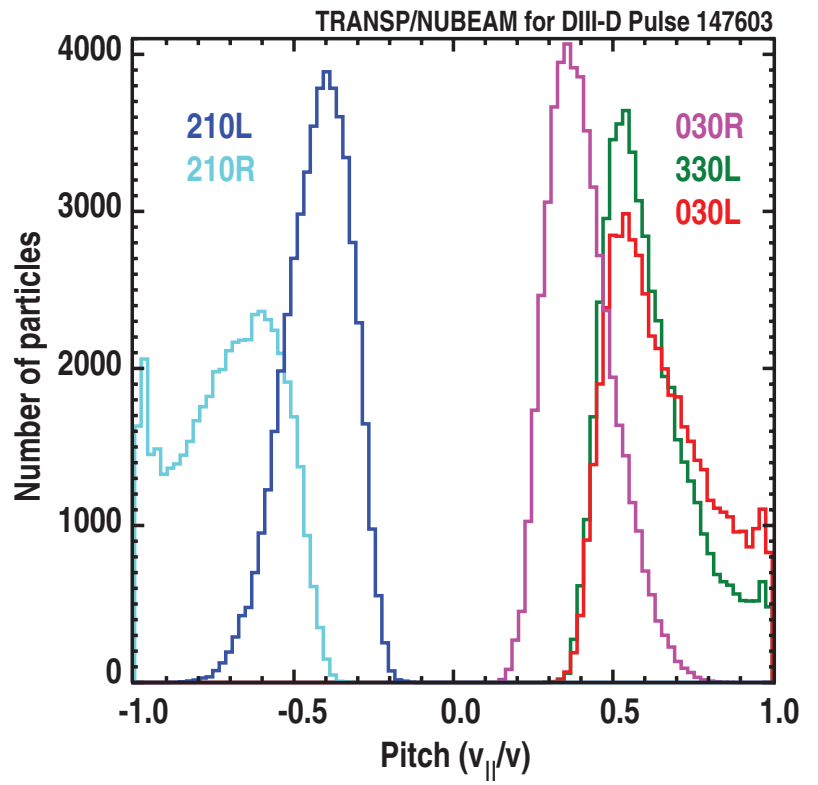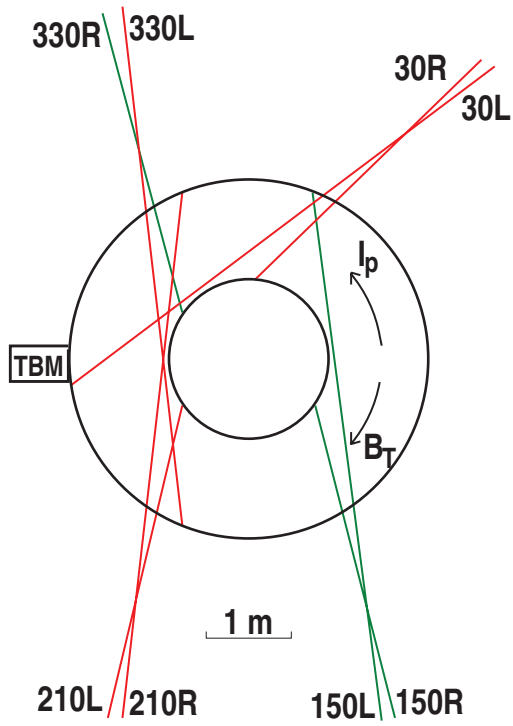Tile 4

G.J. Kramer   Figure 1

Figure 1 (f1.eps)

(a) NBI no TBM (b) NBI and TBM (c) ECRH and TBM

Heat load (MW/m²)

1.0

0.0

G.J. Kramer   Figure 2

Figure 2 (f2.eps)

TRANSP/NUBEAM for DIII-D Pulse 147603

G.J. Kramer   Figure 3

Figure 3 (f3.eps)

Tangential beams

Heat load: 0.0 — 13.0 MW/m²

Co-current

9.1 MW/m²
EXP. 330L+0.5*030L

6.7 MW/m²
ASCOT 330L+0.5*030L

8.2 MW/m²
OFMC 330L+0.5*030L

5.1 MW/m²
SPIRAL 330L+0.5*030L

Counter-current

7.4 MW/m²
EXP. 210R+0.5*030L

9.3 MW/m²
ASCOT 210R+0.5*030L

8.2 MW/m²
OFMC 210R+0.5*030L

5.1 MW/m²
SPIRAL 210R+0.5*030L

Vertical height (m)

Toroidal angle (deg)
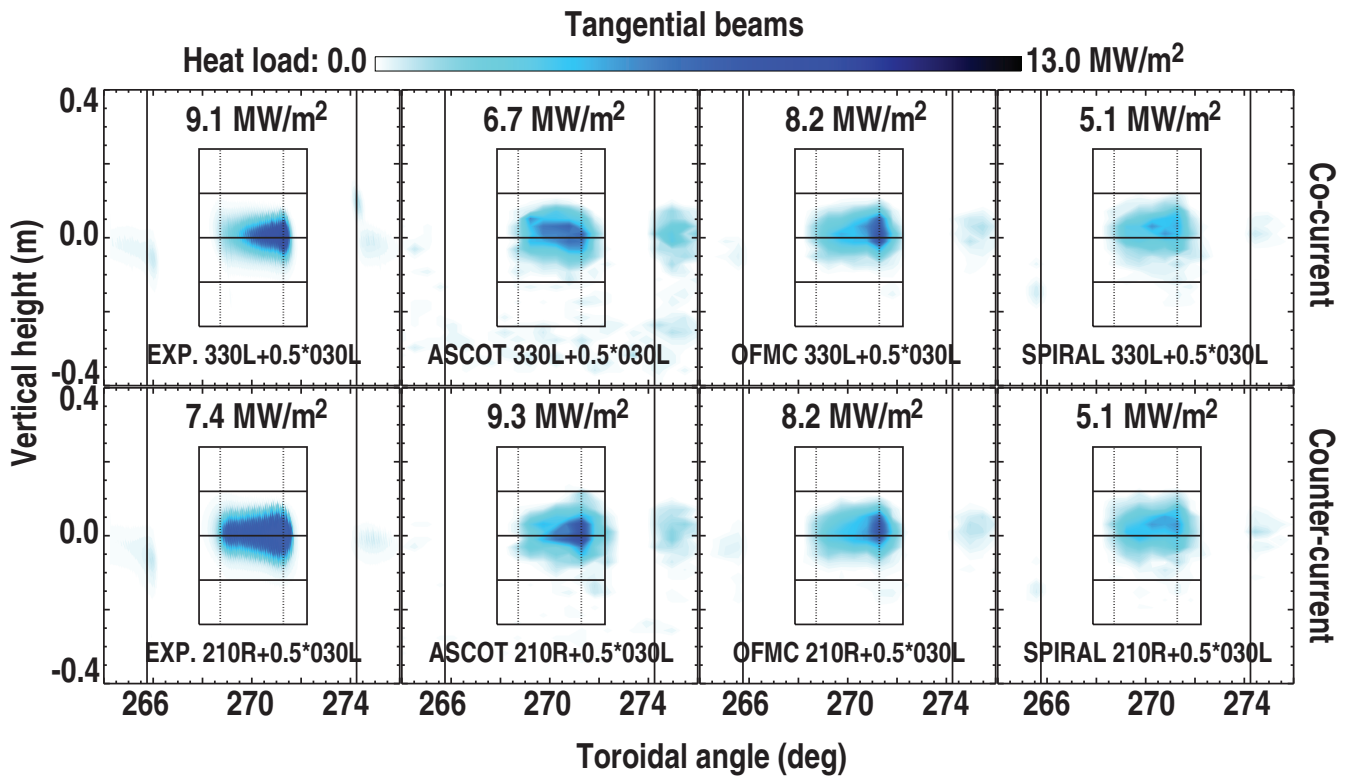
G.J. Kramer　　　　　　Figure 4

Figure 4 (f4.eps)

Perpendicular beams

Heat load: 0.0 — 13.0 MW/m²

Co-current

8.7 MW/m² — EXP. 030R+0.5*030L

8.3 MW/m² — ASCOT 030R+0.5*030L

10.6 MW/m² — OFMC 030R+0.5*030L

6.3 MW/m² — SPIRAL 030R+0.5*030L

Counter-current

7.9 MW/m² — EXP. 210L+0.5*030L

6.9 MW/m² — ASCOT 210L+0.5*030L

12.7 MW/m² — OFMC 210L+0.5*030L

8.5 MW/m² — SPIRAL 210L+0.5*030L

Vertical height (m)

Toroidal angle (deg)
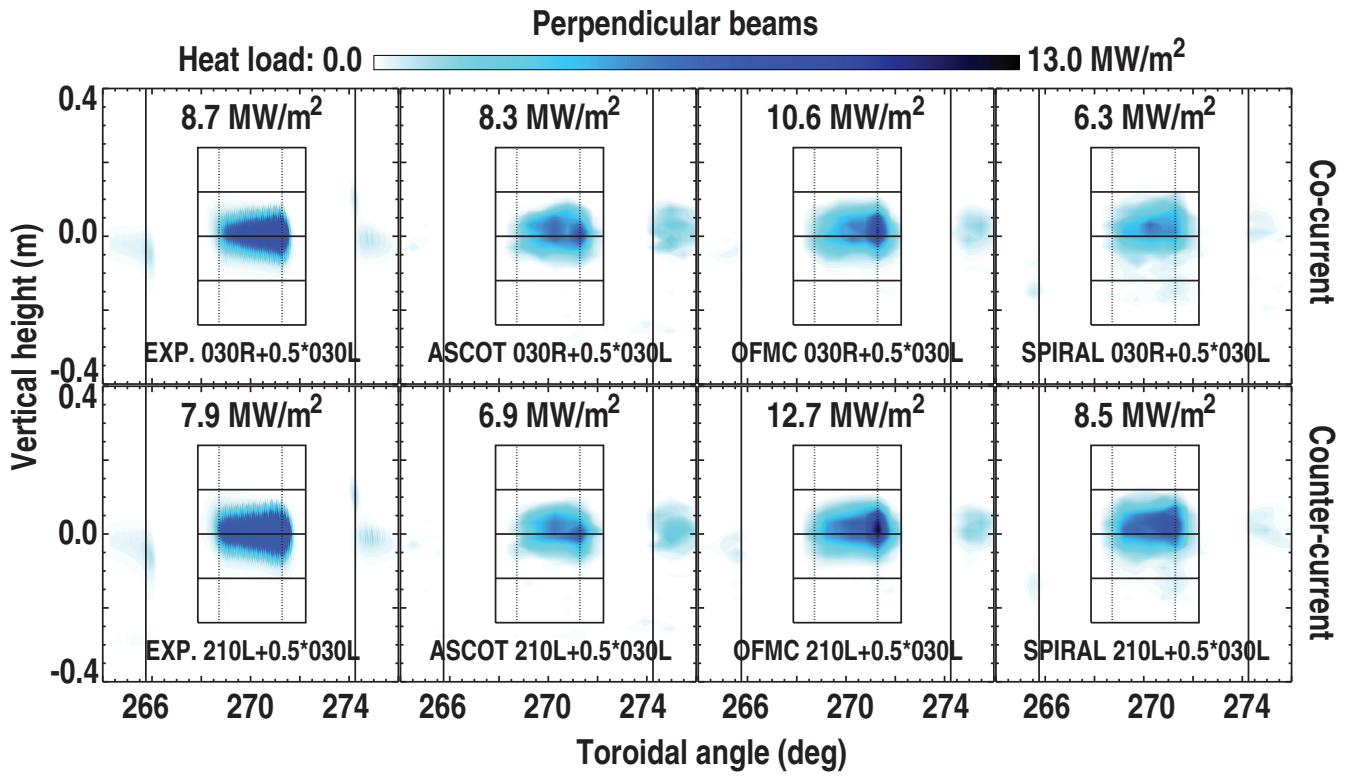
G.J. Kramer   Figure 5

Figure 5 (f5.eps)
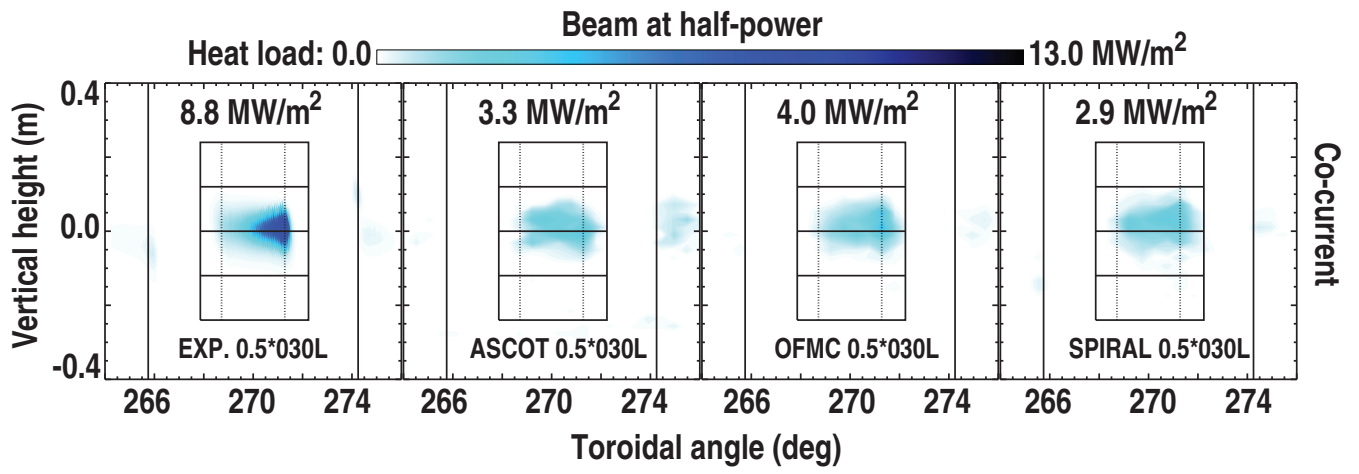
G.J. Kramer   Figure 6

Figure 6 (f6.eps)
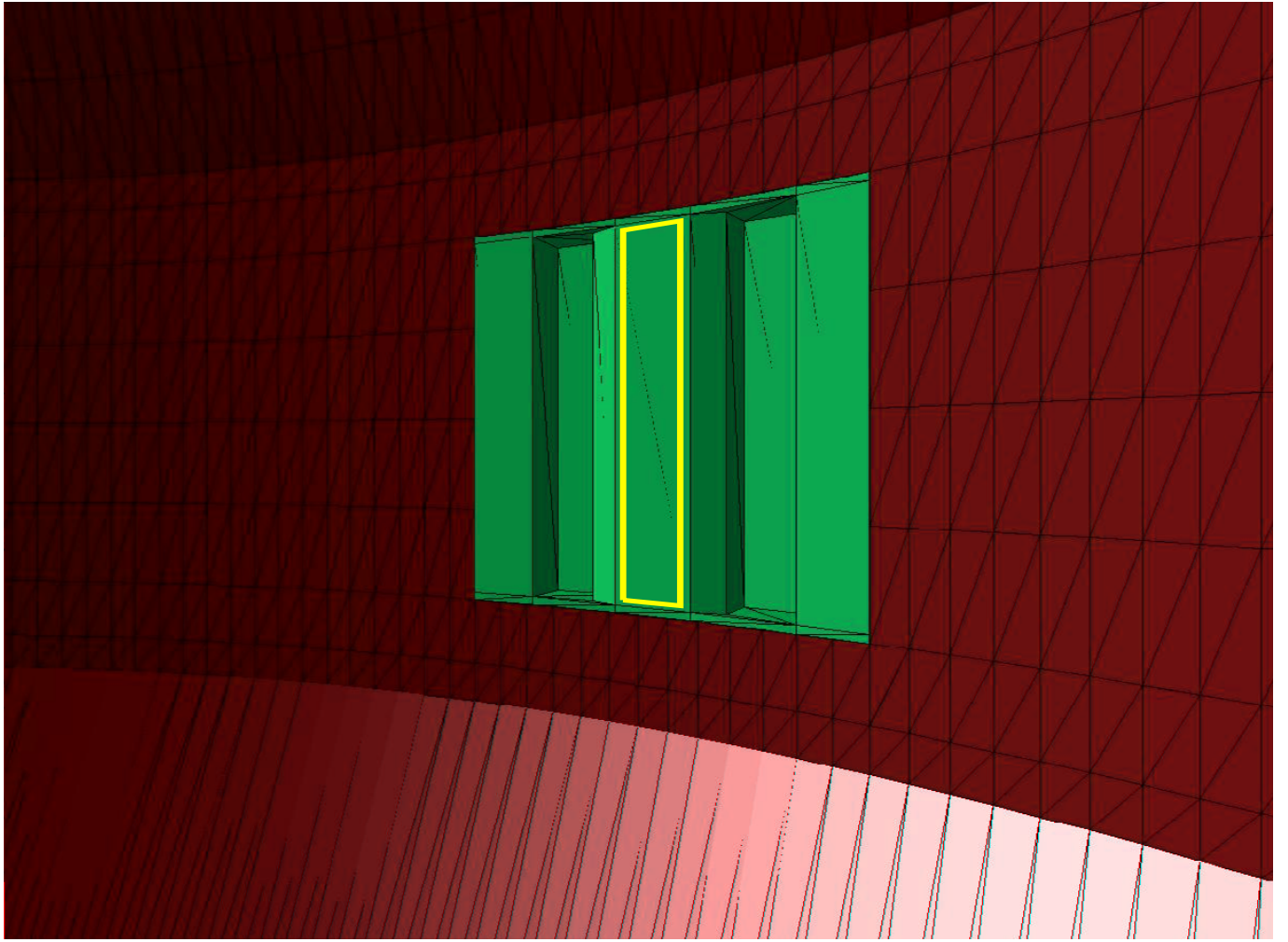
Figure 7 (f7.ps)
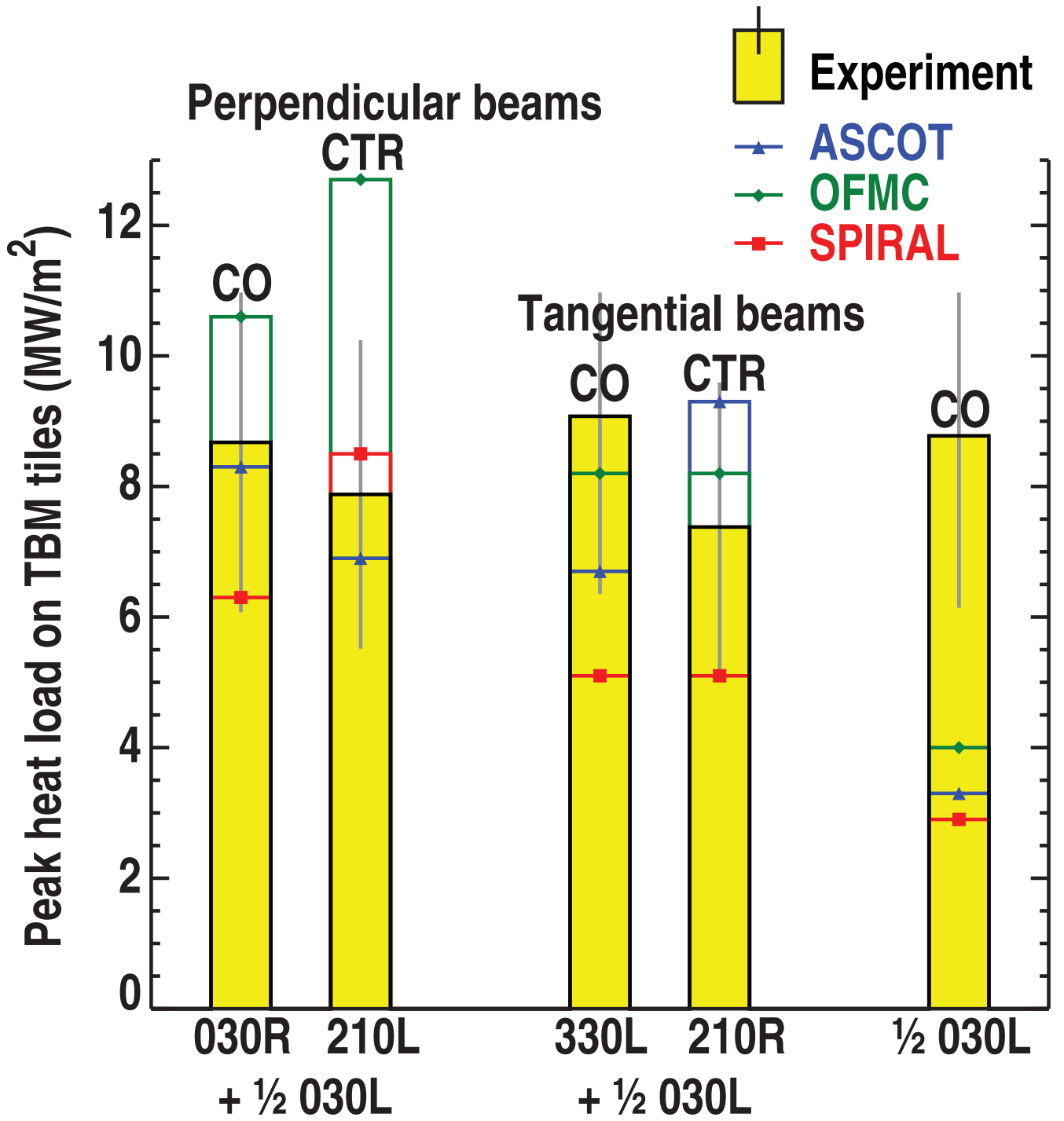
G.J. Kramer   Figure 8

Figure 8 (f8.eps)
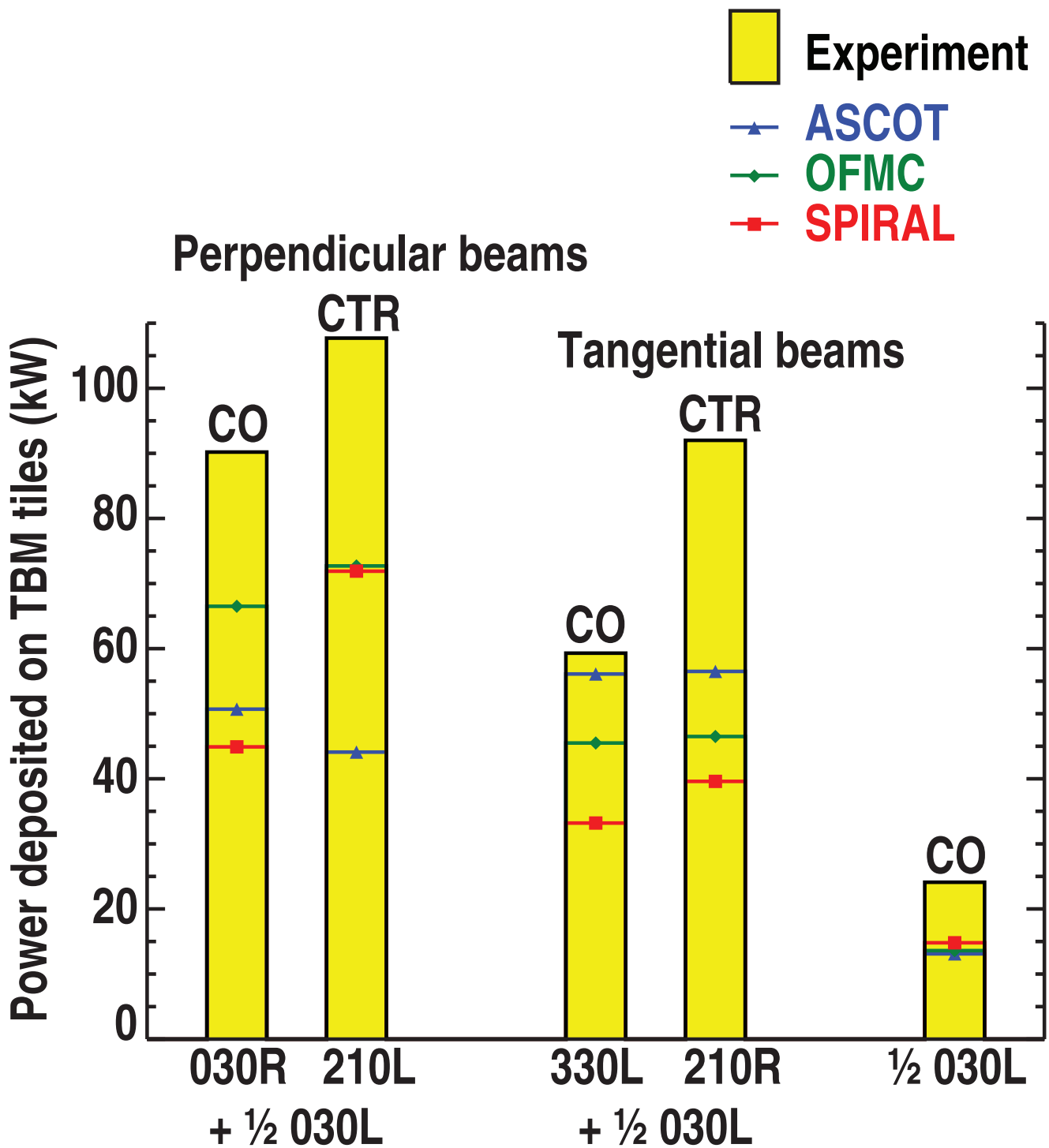
G.J. Kramer   Figure 9

Figure 9 (f9.eps)

Information Services
Princeton Plasma Physics Laboratory
P.O. Box 451
Princeton, NJ 08543

Phone: 609-243-2245
Fax: 609-243-2751
e-mail: pppl_info@pppl.gov
Internet Address: http://www.pppl.gov